

---

# Very Deep Graph Neural Networks Via Noise Regularisation

---

**Jonathan Godwin** \*  
DeepMind

**Michael Schaarschmidt**  
DeepMind

**Alexander Gaunt**  
DeepMind

**Alvaro Sanchez-Gonzalez**  
DeepMind

**Yulia Rubanova**  
DeepMind

**Petar Veličković**  
DeepMind

**James Kirkpatrick**  
DeepMind

**Peter Battaglia**  
DeepMind

## Abstract

Graph Neural Networks (GNNs) perform learned message passing over an input graph, but conventional wisdom says performing more than handful of steps makes training difficult and does not yield improved performance. Here we show the contrary. We train a deep GNN with up to 100 message passing steps and achieve several state-of-the-art results on two challenging molecular property prediction benchmarks, Open Catalyst 2020 IS2RE and QM9. Our approach depends crucially on a novel but simple regularisation method, which we call “Noisy Nodes”, in which we corrupt the input graph with noise and add an auxiliary node autoencoder loss if the task is graph property prediction. Our results show this regularisation method allows the model to monotonically improve in performance with increased message passing steps. Our work opens new opportunities for reaping the benefits of deep neural networks in the space of graph and other structured prediction problems.

## 1 Introduction

Advances in the ability to successfully train very deep neural networks have been key to improving performance in image recognition, language modeling, and many other domains [35, 40, 50, 29, 25, 13]. Graph Neural Networks (GNNs) are a family of deep networks that operate on graph structured data by iteratively passing learned messages over the graph’s structure [47, 12, 23, 7]. While GNNs are very effective in a wide variety of tasks [61, 56, 5], deep GNNs, which perform more than 5-10 message passing steps, have not typically yielded better performance than shallower GNNs [38, 60, 62]. While in principle deep GNNs should have greater expressivity and ability to capture complex functions, it has been proposed that in practice “oversmoothing” [17] and “bottleneck effects” [1] limit the potential benefits of deep GNNs. The purpose of this work is to reap the benefits of deep GNNs while avoiding such limitations.

Oversmoothing is a proposed phenomenon where a GNN’s latent node representations become increasing similar over successive steps of message passing [17]. Once these representations are oversmoothed, adding further steps does not add expressive capacity, and so performance does not improve. Bottleneck effects are thought to limit the ability of a deep GNN to communicate information over long ranges, because as the number of steps increases and causes the receptive

---

\*Correspondence to jonathangodwin@deepmind.com.

fields to grow, the intermediate nodes must propagate information between larger and larger sets of peripheral nodes, limiting the ability to precisely transmit individual pieces of information [1]. We speculate that these are reasons why previous strong GNN results on the molecular property benchmarks we study here, Open Catalyst 2020 (OC20) [16] and QM9 [42], report depths of only 4 [31] and 8 [11], even with large hyperparameter searches.

Originally we trained a very deep GNN and, like previous work, we found negligible benefits from increasing depth on OC20 and QM9. However, we then developed a noise regularisation approach, which we term “Noisy Nodes”, which provides dramatic improvements in performance: we found increasing the GNN’s depth monotonically decreased error. During training, our noise regularisation approach corrupts the input graph’s nodes with noise, and then adds an autoencoding loss if a node prediction task is not defined. We posit that our Noisy Nodes approach is effective because the model is rewarded for maintaining and refining distinct node representations through message passing to the final output, which causes it to resist oversmoothing and overfitting. Like denoising autoencoders, it may also encourage the model to explicitly learn the manifold on which the real graphs lie.

Using only atom types and positions, our model improves state-of-the-art (SOTA) performance on the OC20 IS2RE task by 43% over previous work and achieves top results on 4 out of 12 of the QM9 tasks. On OC20 IS2RS our model’s raw performance is currently second behind SOTA, but it runs roughly 400x faster because it directly predicts the target rather than using the iterative relaxation technique previous models use. Moreover, there is nothing specific to molecules or 3D geometries in our regulariser—the Noisy Nodes technique can be applied to a wide range of graph prediction problems and has potential to make deep GNNs more generally valuable, analogous to how depth often uniquely benefits others neural network architectures.

## 2 Related Work

**Scaling Graph Neural Networks with Depth.** Recent work has aimed to understand why it is challenging to realise the benefits of training very deep GNNs [57]. A key contribution has been the analysis of “oversmoothing” which describes how all node features become almost identical in GCNs after a few layers. Since first being noted in [38] oversmoothing has been studied extensively and regularisation techniques have been suggested to overcome it [17, 15, 43, 62, 58], but these studies have not shown consistent improvements as depth increases. Another insight has been the analysis of the bottleneck effect in Alon and Yahav [1] which may be alleviated by using a fully connected graph. Finally, deep GNNs have been trained using techniques developed for CNNs [36, 37], but with no conclusive improvement from depth.

**Machine Learning for Molecular Property Prediction.** One application of GNNs is to speed up quantum chemistry calculations which operate on a graph structured representation of a molecule [21, 23, 48, 28]. In these graphs atoms are nodes and edges are constructed between close neighbours. Common goals are the prediction of molecular properties [42], forces [19], energies [16] and charges [53]. These datasets have spurred the development of GNNs that embed 3D physical symmetry inductive biases such as the rotation equivariance of forces. Such inductive biases typically improve performance and sample complexity.

A common approach to embed physical symmetries is to design a network that predicts a rotation and translation invariant energy [48, 31, 39]. The derivatives of such a model with respect to its positions are energy conserving rotation equivariant forces. The input features of such models include distances [48], angles [32, 31] or torsions and higher order terms [39]. As higher order terms such as angles are added the size of the input representation can increase significantly [32], and therefore the memory and compute requirements of the model.

An alternative approach to embedding symmetries is to design a rotation equivariant neural network that predicts quantities such as forces directly [52, 34, 33, 22, 8, 2, 46]. However, the benefits of such models are typically seen on smaller data (e.g. Satorras et al. [46]), and such approaches have yet to achieve SOTA performance on large quantum chemistry datasets. Not all competitive models embed rotation symmetries—notably ForceNet [28] does not enforce rotation equivariance.

**Denoising Models.** Training neural networks with noise has a long history [49, 9]. Of particular relevance are Denoising Autoencoders [54] in which an autoencoder is trained to map corrupted inputs  $\tilde{x}$  to uncorrupted inputs  $x$ . Denoising Autoencoders have found particular success as a form of

pre-training for representation learning [55]. More recently, in research applying GNNs to simulation [44, 45, 41] Gaussian noise is added during training to input positions of a ground truth simulator to mimic the distribution of errors of the learned simulator. Pre-training methods [20, 59, 51] are another similar approach; most similarly to our method Hu et al. [27] apply a reconstruction loss to graphs with masked nodes to generate graph embeddings for use in downstream tasks.

### 3 Model

#### 3.1 Graph prediction problem definition

Let  $G = (V, E, g)$  be an input graph. The nodes are  $V = \{v_1, \dots, v_{|V|}\}$ , where  $v_i \in \mathbb{R}^{d_v}$ . The directed, attributed edges are  $E = \{e_1, \dots, e_{|E|}\}$ : each edge includes a sender node index, receiver node index, and edge attribute,  $e_k = (s_k, r_k, e_k)$ , respectively, where  $s_k, r_k \in \{1, \dots, |V|\}$  and  $e_k \in \mathbb{R}^{d_e}$ . The graph-level property is  $g \in \mathbb{R}^{d_g}$ .

The goal is to predict a target graph,  $G'$ , with the same structure as  $G$ , but different node, edge, and/or graph-level attributes. We denote  $\hat{G}'$  as a model’s prediction of  $G'$ . Some error metric defines quality of  $\hat{G}'$  with respect to the target  $G'$ ,  $\text{Error}(\hat{G}', G')$ , which the training loss terms are defined to optimize.

#### 3.2 Base GNN Model

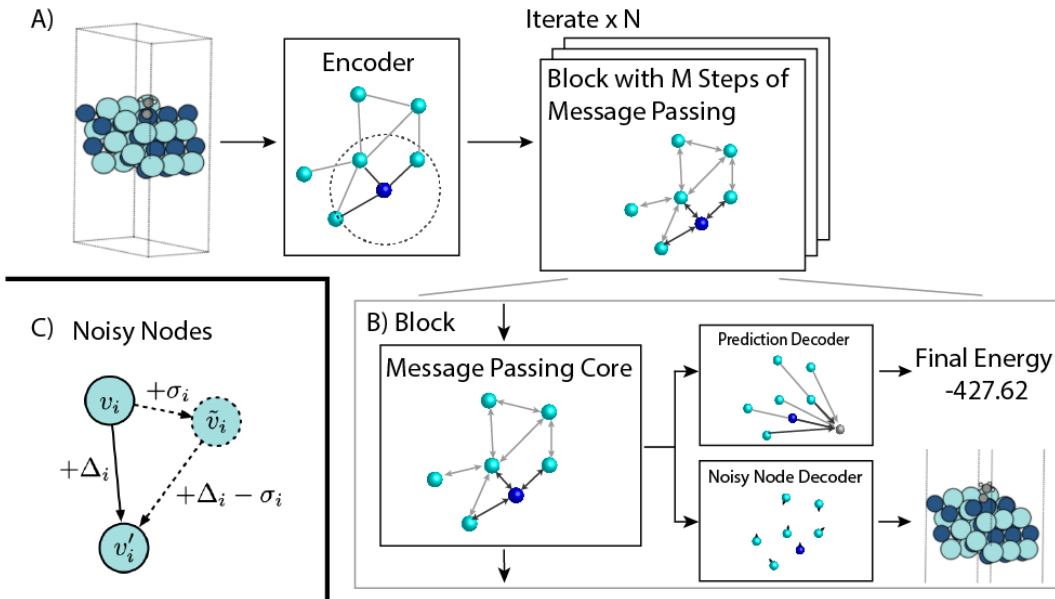


Figure 1: **A) Model Overview.** The system is encoded using Noisy Nodes, and then a graph is constructed by connecting neighboring atoms within a connectivity radius. A block of  $M$  unshared message passing steps is performed  $N$  times, for  $N \times M$  total steps. **B) Block.** Each block consists of  $M$  steps of message passing. During training we decode the output of each block and compute a loss using Noisy Nodes against the same target. We optimise the average of the losses. During evaluation the prediction of the final block is used. **C) Noisy Nodes.** The input  $v_i$  is corrupted with additive noise  $\sigma_i$ . When input  $v_i$  is used as  $v_i'$ , the auxiliary objective amounts to a denoising autoencoder.

Our base model is based on the Graph Net Simulator [45], but modified for molecular tasks and to make graph-level predictions. It operates on 3D points representing the positions of atoms, but apart from featurising interatomic distances using Radial Bessel [32] functions, our model has no other quantum chemistry inspired features.

Our model has three parts the Encoder, the Processor and the Decoder. Let  $a_i \in V$  be the set of atoms in a molecule (for convenience we use  $a_i$  to represent atom positions in sections concerning 3D

geometry). The Encoder,  $\mathcal{E} : \mathcal{V} \rightarrow \mathcal{G}^0$  maps atoms,  $V \in \mathcal{V}$ , to a latent graph,  $G^{(0)} \in \mathcal{G}^{(0)}$  (the initial encoded latent graph). The Processor,  $\mathcal{P} : \mathcal{G}^{(n)} \rightarrow \mathcal{G}^{(n+1)}$ , passes messages across the latent graph using an Interaction Network [6, 44, 23], and the Decoder  $\mathcal{D} : \mathcal{G}^{(N)} \rightarrow \mathcal{G}'$ , where  $G' \in \mathcal{G}'$  represents target graph properties to predict. Here we use  $G' = (\{a^\Delta, \emptyset, g'\}$ , where  $a^\Delta$  are the atoms' position changes from input to target and  $g'$  are molecular properties (the  $\emptyset$  indicates the output graph's edge attributes are ignored). Our network is built from standard building blocks (overview in Figure 1A).

**Encoder.** During training Noisy Nodes is first applied to the atom positions (see Section 3.3 below). Then our encoder constructs a latent graph with a node per atom and adding edges between nodes within a "connectivity radius",  $R$ , which reflects the local interactions of atoms. Edges are computed using a k-nearest neighbors algorithm after noise has been applied to edges.

The node features are a learned embedding lookup of the atom type, and in the case of OC20 two additional binary features representing whether the atom is part of the adsorbate or catalyst and whether the atom remains fixed during the quantum chemistry simulation.

The edge features,  $e_k$  are the distances  $|d|$  featurised using  $c$  Radial Bessel basis functions,  $\tilde{e}_{RBF,c} = \sqrt{\frac{2}{R}} \frac{\sin(\frac{c\pi}{R}d)}{d}$ , and the edge vector displacements,  $d$ , normalised by the edge distance:

$$e_k = \text{Concat}(\tilde{e}_{RBF,1}(|d|), \dots, \tilde{e}_{RBF,c}(|d|), \frac{d}{|d|})$$

Where  $d = a_{s_k} - a_{r_k}$ . Note that since this encoding does not have absolute atom positions as an input it is translation invariant by construction.

**Processor.** The processor consists of "blocks", where each block contain a stack of Interaction Networks (each one known as a "message passing layer") with identical structure but different weights. The node and edge functions are 3 layer MLPs activated with shifted softplus ( $ssp(x) = \ln(0.5e^x + 0.5)$ , [48]), followed by layer normalisation [3]. Residual connections on both the nodes and edges are added to each message passing layer. We recurrently apply each block, a process we call "block iteration". We calculate the number of message passing layers by multiplying the number of blocks by the block size, for example 10 applications of a block of size 10 corresponds to 100 ( $10 \times 10$ ) message passing layers.

**Decoder.** The decoder consists of two parts, a *graph-level decoder* which predicts a single output for the input graph, and a *node-level decoder* which predicts individual outputs for each node. The graph-level decoder implements the following equation:

$$y = W^{\text{Proc}} \sum_{i=1}^{|V|} \text{MLP}_{\text{Proc}}(a_i^{\text{Proc}}) + b^{\text{Proc}} + W^{\text{Enc}} \sum_{i=1}^{|V|} \text{MLP}_{\text{Enc}}(a_i^{\text{Enc}}) + b^{\text{Enc}}$$

Where  $a_i^{\text{Proc}}$  are node latents from the Processor,  $a_i^{\text{Enc}}$  are node latents from the Encoder,  $W^{\text{Enc}}$  and  $W^{\text{Proc}}$  are linear layers,  $b^{\text{Enc}}$  and  $b^{\text{Proc}}$  are biases, and  $|V|$  is the number of nodes. The node-level decoder is simply an MLP applied to each  $a_i^{\text{Proc}}$  which predicts  $a_i^\Delta$ .

### 3.3 Our Noisy Nodes Regularisation Technique

We add the Noisy Nodes regulariser to our base model operating on 3D points. The Noisy Nodes loss has two components. First, we add noise to the input graph. Second, we add a node or edge level autoencoder auxiliary loss if the task is graph property prediction. Here we focus on 3D spatial problems, where noise is added to nodes which represent positions, but our technique can be applied to generally to the edges, nodes, or graph-level input features, and they need not be in  $\mathbb{R}^d$ .

The Noisy Nodes method modifies the original problem definition above in several ways. It introduces a graph corrupted by noise,  $\tilde{G} = (\tilde{V}, \tilde{E}, \tilde{g})$ , where  $\tilde{v}_i \in \tilde{V}$  is constructed by adding noise,  $\sigma_i$ , to the input nodes,  $\tilde{v}_i = v_i + \sigma_i$ . The edges,  $\tilde{E}$ , and graph-level attribute,  $\tilde{g}$ , can either be uncorrupted by noise (i.e.,  $\tilde{E} = E$ ,  $\tilde{g} = g$ ), calculated from the noisy nodes (for example in a nearest neighbors graph), or corrupted independent of the nodes—these are minor choices that can be informed by the specific problem setting.

Our method also requires a node level target. For problems where the Error is defined with respect to graph-level predictions (e.g., predict the minimum energy value of some molecular system), a second output head can be added to the GNN architecture which requires denoising the noisy inputs as node-level targets, analogous to an auxiliary denoising autoencoder head and training objective. In other words, because the  $v'_i \in V'$  is not specified by the goal, we can set  $v'_i = v_i$  and train the model to predict the uncorrupted input nodes.

Alternatively, if the Error is defined with respect to node-level predictions, (e.g. predict the positions of atoms at their minimum energy state), it is possible to train the model to map directly from corrupted node inputs to targets. In our case, we use relative node targets [41] to enforce translation invariance. Relative targets modified for noise become  $v'_i - \tilde{v}_i = v'_i - (v_i + \sigma_i) = \Delta_i - \sigma_i$ . Figure 1B details the various scenarios in a single diagram.

The Noisy Nodes objective helps ameliorate oversmoothing by adding a diverse per-node prediction loss that regularises identical node latents. In addition, using noise corrupted inputs helps prevent overfitting by ensuring that input graphs cannot be memorised.

**The Graph Manifold Learning Perspective.** By using an implicit mapping from corrupted data to correct data, the Noisy Nodes objective encourages the model to learn the manifold on which the correct data lies—the GNN learns to go from low probability graphs to high probability graphs. In the autoencoder case the GNN learns the manifold of the input data. When node targets are provided, the GNN learns the manifold of the target data (e.g. the manifold of atoms at equilibrium). For graphs constructed from points in Euclidean space, such as atoms [42], the manifold may include commonly repeated substructures that are useful for downstream prediction tasks.

## 4 Training

**Loss.** We minimise the mean squared error loss on mean and standard deviation normalised targets in using the Adam [30] optimiser with warmup and cosine decay. Node and edge latents as well as MLP hidden layers were sized 512, with 3 layers per MLP and using shifted softplus activations throughout. Models were trained on 8 TPU devices and evaluated on V100 GPUs. QM9 models were trained for up to 24 hours, and OC models for up to 200 hours. We provide the full set of hyper-parameters and computational resources used separately for each dataset in the Appendix.

Our model is implemented in JAX using Haiku and Jraph for GNNs, and Optax for training [10, 4, 24, 26]. We found that computing and averaging the loss over each block application improves training stability and gives a small improvement in performance. Model selection used early stopping.

## 5 Experiments and Results

We tested our model on two challenging molecular property prediction benchmarks: OC20 [16] and QM9 [42]. These benchmarks are detailed below, but as general distinctions, OC20 uses graphs 2-20x larger than QM9, and so we expected greater benefits on OC20 from deeper message passing. Also, while QM9 always requires graph-level prediction, one of OC20’s two tasks (IS2RS) requires node-level predictions while the other (IS2RE) requires graph-level predictions.

### 5.1 Open Catalyst 2020

**Dataset.** The OC20 dataset [16] (CC Attribution 4.0) describes the interaction of a small molecule (the adsorbate) and a large slab (the catalyst), with total systems consisting of 20-200 atoms. The data is generated using a process called "atomic relaxation" which uses a second order optimisation method (e.g. [14]) to minimise the energy of a system with respect to atom positions. In total, the dataset consists of 1m+ atomic relaxation trajectories, constructed from 70 million hours of Density Functional Theory (DFT) calculations, with an average relaxation trajectory length of 200.

We focus on two of the community challenges; the Initial Structure to Resulting Energy (IS2RE) task which takes the initial structure of the relaxation and predicts the energy at the relaxed state, and the Initial Structure to Resulting Structure (IS2RS) which takes the initial structure and predict the relaxed state structure. These are both very challenging tasks with benchmark relative errors far higher than those seen on QM9.

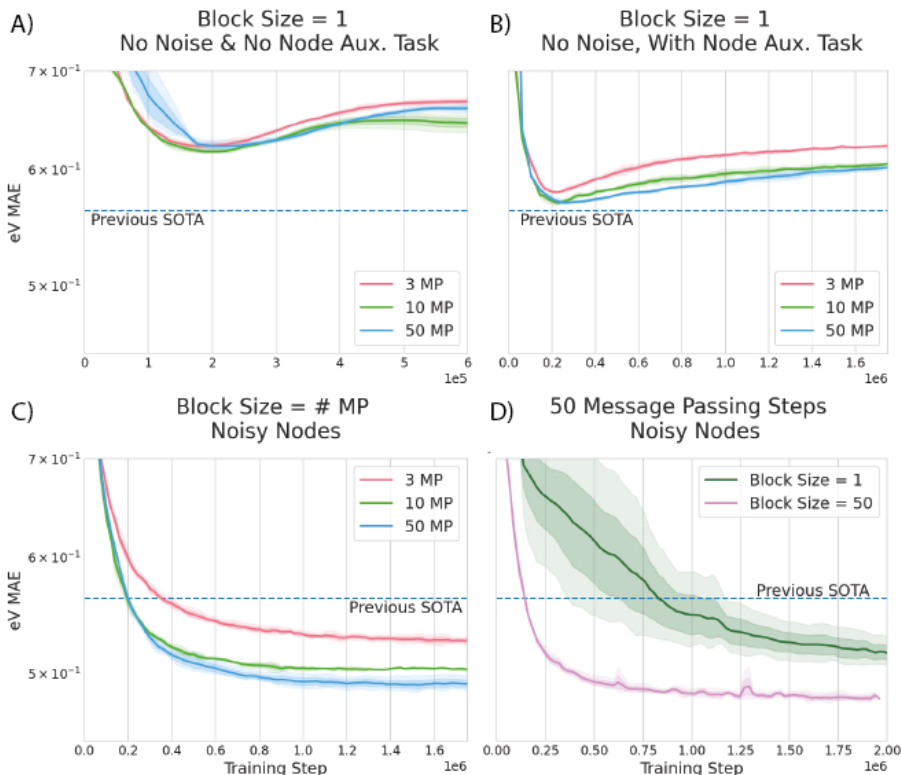


Figure 2: Validation curves on OC20 IS2RE ID. **A)** Without any node targets our model has poor performance and realises no benefit from depth, reflecting commonly held views about scaling GNNs. **B)** After adding a position node loss, we see performance improves as the number of message passing layers increases even with the same number of parameters. However, we still see overfitting. **C)** As we add Noisy Nodes the model achieves SOTA and stops overfitting. **D)** Adding Noisy Nodes allows a model with block size 1 to achieve SOTA. Note in these charts "block size" is the number of message passing layers in a block.

One of the goals of the OC20 dataset is to stimulate the development a model that can be applied to catalyst screening. In order to do this the authors estimate a model must make predictions in 10 ms [16]. For that reason in IS2RS we train a model to directly predict the resulting structure, rather than using a relaxation. If we assume that each iteration requires 2x the compute of a single forward pass to compute the derivative, and that each relaxation consists of 200 steps then predicting IS2RS using a relaxation is 400x more expensive than a single forward pass.

Models are evaluated on 4 held out test sets; a set of In Distribution (ID) catalysts and adsorbates, Out of Distribution (OOD) catalysts and ID adsorbates, ID catalysts and OOD adsorbates and finally a set of both OOD catalysts and adsorbates. Four canonical validation datasets are also provided. Test sets are evaluated on a remote server hosted by the dataset authors with a very limited number of submissions per team.

**Source of Noise for Noisy Nodes.** For OC20 we have access to intermediate 3D states along a relaxation trajectory, which provide a form of structured noise for Noisy Nodes. During training we first sample from a point in this relaxation trajectory, and then add I.I.D Gaussian noise with mean zero and  $\sigma^2 = 0.3$ . The Noisy Node target is the relaxed structure.

**Additional Training Details.** OC20 provides the periodic axes of the ground truth DFT simulation. We use these by first transforming the inputs to the periodic basis, apply the model there, and then transform back to the input co-ordinate system:  $A(\text{GNN}(A^{-1}\nu))$  where  $\nu$  is the matrix of atom positions and  $A$  is the transformation matrix. In addition we append the following rotation and translation invariant vector  $(\alpha\beta^T, \beta\gamma^T, \alpha\gamma^T, |\alpha|, |\beta|, |\gamma|) \in \mathbb{R}^6$  to the edge features where  $\alpha, \beta, \gamma$  are vectors of the transformation matrix. This additional vector provides rotation invariant angular and extent information to the GNN.

Table 1: OC20 ISRE Validation Set Ablations, eV MAE, ↓. Mean and Standard Deviation of 3 seeds reported. N×M indicates N repetitions of a block of size M.

Model	Block Size	OOD Both	OOD Adsorbate	OOD Catalyst	ID
No Noise	1 × 50	0.59 ±0.01	0.65 ±0.01	0.55 ±0.00	0.54 ±0.00
Noisy Nodes	50 × 1	0.49 ±0.00	0.54 ±0.00	0.51 ±0.01	0.51 ±0.01
Noisy Nodes	1 × 50	0.48 ±0.00	0.53 ±0.00	0.49 ±0.01	0.48 ±0.00
Noisy Nodes	5 × 10	0.47±0.00	0.52 ±0.00	0.48 ±0.00	0.47 ±0.00
Noisy Nodes	10 × 10	<b>0.46</b> ±0.00	<b>0.51</b> ±0.00	<b>0.48</b> ±0.00	<b>0.47</b> ±0.00

Table 2: Results on OC20 IS2RE Test

eV MAE ↓				
	SchNet	DimeNet++	SphereNet	Noisy Nodes
OOD Both	0.704	0.661	0.638	<b>0.504 (-21.0%)</b>
OOD Adsorbate	0.734	0.725	0.703	<b>0.565 (-19.6%)</b>
OOD Catalyst	0.662	0.576	0.571	<b>0.493 (-13.7%)</b>
ID	0.639	0.562	0.563	<b>0.478 (-15.1%)</b>
Average Energy within Threshold (ADwT) ↑				
	SchNet	DimeNet++	SphereNet	Noisy Nodes
OOD Both	0.0221	0.0241	0.0241	<b>0.0382 (+58.5%)</b>
OOD Adsorbate	0.0233	0.0207	0.0229	<b>0.0349 (+52.4%)</b>
OOD Catalyst	0.0294	0.0410	0.0409	<b>0.0550 (+34.5%)</b>
ID	0.0296	0.0425	0.0447	<b>0.0571 (+27.7%)</b>

**IS2RE Results.** In Figure 2 we show that depth improves performance for IS2RE. Figure 2 A) shows that without using the any node auxiliary targets there is no benefit to be gained adding depth. However, once the Noisy Nodes objective is used, performance increases monotonically as depth increases. Furthermore, Figure 2 D) shows our model can achieve SOTA with a single message passing step recurrently applied 50 times.

In Table 1 we conduct an ablation on our hyperparameters and find again that using Noisy Nodes allows us to realise the benefits of depth. Interestingly we find that increased parameter counts do not necessarily improve performance—our best model was a block of 10 message passing steps recurrently applied 10 times. Moreover, block iteration is computationally more efficient than running a single large block with the same number of message passing steps (typically requiring half the training time). Results were averaged over 3 seeds and standard errors on the best obtained checkpoint show little sensitivity to initialisation. Further analysis of the effect of Noisy Nodes on GNN activations can be found in the Appendix.

Our best model on IS2RE was a 100 layer GNN with a block size of 10 × 10 which achieved a 43.3% relative performance improvement against SOTA results (Table 2). Due to limited permitted test submissions, results presented here were from one test upload of our best performing validation seed.

Table 3: OC20 IS2RS Validation, ADwT, ↑

Model	Block Size	OOD Both	OOD Adsorbate	OOD Catalyst	ID
No Noise	1 × 50	43.0%±0.0	38.0%±0.0	37.5% 0.0	40.0%±0.0
Noisy Nodes	50 × 1	49.2%±0.0	42.6%±0.0	42.5%±0.0	43.6% ±0.01
Noisy Nodes	1 × 50	50.1%±0.0	44.3%±0.0	44.1%±0.0	46.1% ±0.0
Noisy Nodes	5 × 10	52.0%±0.0	46.2%±0.0	46.1% ±0.0	48.3% ±0.0
+ Pos only	5 × 10	53.7%±0.0	47.8%±0.0	47.6% ±0.0	50.0% ±0.0
+ Pos only	10 × 10	<b>54.3%</b> ±0.0	<b>48.3%</b> ±0.0	<b>48.2%</b> ±0.0	<b>50.0%</b> ±0.0

Table 4: OC20 IS2RS Test, ADwT,  $\uparrow$ 

Model	Method	OOD Both	OOD Adsorbate	OOD Catalyst	ID
SchNet	Relaxation	15.3%	13.2%	14.6%	15.7%
DimeNet++	Relaxation	32.3%	26.7%	30.1%	30.7%
Force Only	Relaxation	53.1%	45.2%	48.6%	48.8%
Large Force Only	Relaxation	<b>54.8%</b>	<b>48.5%</b>	<b>51.0%</b>	<b>52.5%</b>
Noisy Nodes	Direct	52.5%	43.7%	47.8%	50.0%

**IS2RS.** In Table 3 we perform the same ablation studies on the IS2RS validation set using the Average Distance within Threshold (ADwT) metric and observe the same relative effects. In Table 4 we see that our model reaches comparable performance to relaxation approaches on the IS2RS test set on ADwT. Additional metrics reported by the leaderboard server can be found in the Appendix.

We note a drop between the validation and test sets, which we speculate is due to distribution shift. We also notice a consistent pattern that having energy predictions as an auxiliary loss inhibits both relaxation and direct position predictions, we speculate that adding more capacity to the positional decoder head may help ameliorate such effects but leave that to future work.

To our knowledge this is the first time a model has been trained to directly predict relaxed structures from initial positions. These results demonstrate the exciting potential of learned models to make as accurate predictions as relaxation approaches, but with 400x less compute.

## 5.2 QM9

**Dataset.** The QM9 benchmark [42] contains 134k molecules in equilibrium with up to 9 heavy C, O, N and F atoms, targeting 12 associated chemical properties (License: CCBY 4.0). We use 114k molecules for training, 10k for validation and 10k for test. All results are on the test set. We subtract a fixed per atom energy from the target values computed from linear regression to reduce variance.

We perform training in eV units for energetic targets, and evaluate using MAE. We summarise the results across the targets using mean standardised MAE (std. MAE) in which MAEs are normalised by their standard deviation, and mean standardised logMAE. Std. MAE is dominated by targets with high relative error such as  $\Delta\epsilon$ , whereas logMAE is sensitive to outliers such as  $\langle R^2 \rangle$ . As is standard for this dataset, a model is trained separately for each target but with identical hyper parameters.

**Source of Noise for Noisy Nodes.** For this dataset we add I.I.D Gaussian noise with mean zero and  $\sigma = 0.02$  to the input atom positions. A denoising autoencoder loss is used.

**Results.** In Table 2 we can see that adding the denoising objective significantly improves results by 23.1% relative. Furthermore increased depth monotonically increases performance.

Our best model is a 30 layer network with block size  $3 \times 10$ , which achieves SOTA on 4 of the 12 targets (SphereNet is the only other model that achieves SOTA on 4 of 12) and comparable performance on the remainder (Table 5). On the std. MAE aggregate metric our model performs better than all other reported results, and is thus SOTA. This is despite having no equivariance or invariance symmetries, or hand crafted molecular features.

$\langle R^2 \rangle$ , the electronic spatial extent, is an outlier for our model. Interestingly, we found that without noise our model achieves 0.33 for this target. We speculate that this target is particularly sensitive to noise, and the best noise value would be significantly lower than for the dataset as a whole.

## 5.3 Limitations

Depth can have diminishing returns. Since training additional layers incurs computational overhead, practitioners must identify the appropriate layer count to achieve optimal performance.

Our method has also not been demonstrated in the small data regime on datasets such as MD17 [19], a regime in which models such as DimeNet++ perform well. This regime has particular importance for learning interatomic potentials since highly accurate experimental data is typically small.



Table 5: QM9, Best Noisy Nodes, Test MAE, Mean &amp; Standard Deviation of 3 Seeds Reported.

Target	Unit	SchNet	EGNN	DimeNet++	SphereNet	Noisy Nodes
$\mu$	D	0.033	0.029	0.030	0.027	<b>0.025</b> $\pm$ 0.01
$\alpha$	$a_0^3$	0.235	0.071	<b>0.043</b>	0.047	0.052 $\pm$ 0.00
$\epsilon_{\text{HOMO}}$	meV	41	29.0	24.6	23.6	<b>20.4</b> $\pm$ 0.2
$\epsilon_{\text{LUMO}}$	meV	34	25.0	19.5	18.9	<b>18.6</b> $\pm$ 0.4
$\Delta\epsilon$	meV	63	48.0	32.6	32.3	<b>28.6</b> $\pm$ 0.1
$\langle R^2 \rangle$	$a_0^2$	<b>0.07</b>	0.11	0.33	0.29	0.70 $\pm$ 0.01
ZPVE	meV	1.7	1.55	1.21	<b>1.12</b>	1.16 $\pm$ 0.01
$U_0$	meV	14.00	11.00	6.32	<b>6.26</b>	7.30 $\pm$ 0.12
$U$	meV	19.00	12.00	<b>6.28</b>	7.33	7.57 $\pm$ 0.03
$H$	meV	14.00	12.00	6.53	<b>6.40</b>	7.43 $\pm$ 0.06
$G$	meV	14.00	12.00	<b>7.56</b>	8.0	8.30 $\pm$ 0.14
$c_v$	$\frac{\text{cal}}{\text{mol K}}$	0.033	0.031	0.023	<b>0.022</b>	0.025 $\pm$ 0.00
std. MAE	%	1.76	1.22	0.98	0.94	<b>0.88</b>
logMAE		-5.17	-5.43	-5.67	<b>-5.68</b>	-5.60

Table 6: QM9 Ablation. N $\times$ M means N repetitions of a block of size M.

	Block Size	std. MAE	% Change	logMAE
No Noise	1 $\times$ 10	1.17	-	-5.39
Noise Added to Nodes	1 $\times$ 10	1.16	-0.9%	-5.32
Noisy Nodes	1 $\times$ 10	0.90	-23.1%	-5.58
Noisy Nodes	2 $\times$ 10	0.89	-23.9%	-5.59
Noisy Nodes	3 $\times$ 10	<b>0.88</b>	<b>-24.8%</b>	<b>-5.60</b>

We focused on the generality of our approach, so did not integrate Noisy Nodes with existing molecular prediction models such as DimeNet, SphereNet, etc. We leave such integration to future work, and believe further improvements could be gained.

## 6 Broader impact

**Who may benefit from this work?** Molecular property prediction with deep networks is a fast-growing area with applications across domains such as drug design, catalyst discovery, synthetic biology, and chemical engineering. Noisy Nodes could aid models applied to these domains. We also demonstrate on OC20 that our direct state prediction approach is nearly as accurate as learned relaxed approaches at a small fraction of the computational cost, which may support material design which requires many predictions.

Finally, Noisy Nodes is also a general technique. It could be adapted and applied to many areas in which GNNs are used—for example, knowledge base completion, physical simulation or traffic prediction. We hope that the benefits of training GNNs with depth could be realised in these domains.

**Potential negative impact and reflection.** Enabling the training of very deep GNNs could contribute to global warming. Care should be taken when utilising depth, and we note that Noisy Nodes settings can be calibrated at shallow depth (e.g. a single block). In future work we plan to further investigate depth-efficiency tradeoffs in GNNs.

## 7 Conclusions

In this work we present Noisy Nodes, a general purpose method for training very deep GNNs which is not specific to molecular property prediction. We demonstrate that graph networks of large depth outperform shallower models even on small graphs, such as QM9, and can lead to substantial gains on very difficult datasets such as OC20. Realising the benefits of very deep GNNs opens new opportunities in the space of graph and other structured prediction problems.

## References

- [1] Uri Alon and Eran Yahav. On the bottleneck of graph neural networks and its practical implications. *ArXiv*, abs/2006.05205, 2020.
- [2] Brandon M. Anderson, T. Hy, and R. Kondor. Cormorant: Covariant molecular neural networks. In *NeurIPS*, 2019.
- [3] Jimmy Ba, J. Kiros, and Geoffrey E. Hinton. Layer normalization. *ArXiv*, abs/1607.06450, 2016.
- [4] Igor Babuschkin, Kate Baumli, Alison Bell, Surya Bhupatiraju, Jake Bruce, Peter Buchlovsky, David Budden, Trevor Cai, Aidan Clark, Ivo Danihelka, Claudio Fantacci, Jonathan Godwin, Chris Jones, Tom Hennigan, Matteo Hessel, Steven Kapturowski, Thomas Keck, Iurii Kemaev, Michael King, Lena Martens, Vladimir Mikulik, Tamara Norman, John Quan, George Papamakarios, Roman Ring, Francisco Ruiz, Alvaro Sanchez, Rosalia Schneider, Eren Sezener, Stephen Spencer, Srivatsan Srinivasan, Wojciech Stokowiec, and Fabio Viola. The DeepMind JAX Ecosystem, 2020. URL <http://github.com/deepmind>.
- [5] V. Bapst, T. Keck, Agnieszka Grabska-Barwinska, C. Donner, E. D. Cubuk, S. Schoenholz, A. Obika, Alexander W. R. Nelson, T. Back, D. Hassabis, and P. Kohli. Unveiling the predictive power of static structure in glassy systems. *Nature Physics*, 16:448–454, 2020.
- [6] P. Battaglia, Razvan Pascanu, Matthew Lai, Danilo Jimenez Rezende, and K. Kavukcuoglu. Interaction networks for learning about objects, relations and physics. *ArXiv*, abs/1612.00222, 2016.
- [7] P. Battaglia, Jessica B. Hamrick, V. Bapst, A. Sanchez-Gonzalez, V. Zambaldi, Mateusz Malinowski, Andrea Tacchetti, David Raposo, A. Santoro, R. Faulkner, Çağlar Gülçehre, H. Song, A. J. Ballard, J. Gilmer, George E. Dahl, Ashish Vaswani, Kelsey R. Allen, Charlie Nash, Victoria Langston, Chris Dyer, N. Heess, Daan Wierstra, P. Kohli, M. Botvinick, Oriol Vinyals, Y. Li, and Razvan Pascanu. Relational inductive biases, deep learning, and graph networks. *ArXiv*, abs/1806.01261, 2018.
- [8] Simon Batzner, T. Smidt, L. Sun, J. Mailoa, M. Kornbluth, N. Molinari, and B. Kozinsky. Se(3)-equivariant graph neural networks for data-efficient and accurate interatomic potentials. *ArXiv*, abs/2101.03164, 2021.
- [9] Charles M. Bishop. Training with noise is equivalent to tikhonov regularization. *Neural Computation*, 7:108–116, 1995.
- [10] James Bradbury, Roy Frostig, Peter Hawkins, Matthew James Johnson, Chris Leary, Dougal Maclaurin, George Necula, Adam Paszke, Jake VanderPlas, Skye Wanderman-Milne, and Qiao Zhang. JAX: composable transformations of Python+NumPy programs, 2018. URL <http://github.com/google/jax>.
- [11] Marc Brockschmidt. Gnn-film: Graph neural networks with feature-wise linear modulation. In *ICML*, 2020.
- [12] Michael M Bronstein, Joan Bruna, Yann LeCun, Arthur Szlam, and Pierre Vandergheynst. Geometric deep learning: going beyond euclidean data. *IEEE Signal Processing Magazine*, 34(4):18–42, 2017.
- [13] T. Brown, Benjamin Mann, Nick Ryder, Melanie Subbiah, J. Kaplan, Prafulla Dhariwal, Arvind Neelakantan, Pranav Shyam, Girish Sastry, Amanda Askell, Sandhini Agarwal, Ariel Herbert-Voss, Gretchen Krueger, T. Henighan, R. Child, A. Ramesh, Daniel M. Ziegler, Jeffrey Wu, Clemens Winter, Christopher Hesse, Mark Chen, Eric Sigler, Mateusz Litwin, Scott Gray, Benjamin Chess, J. Clark, Christopher Berner, Sam McCandlish, Alec Radford, Ilya Sutskever, and Dario Amodei. Language models are few-shot learners. *ArXiv*, abs/2005.14165, 2020.
- [14] R. Byrd, Peihuang Lu, J. Nocedal, and C. Zhu. A limited memory algorithm for bound constrained optimization. *SIAM J. Sci. Comput.*, 16:1190–1208, 1995.

- [15] Chen Cai and Yusu Wang. A note on over-smoothing for graph neural networks. *CoRR*, abs/2006.13318, 2020. URL <https://arxiv.org/abs/2006.13318>.
- [16] Lowik Chanussot\*, Abhishek Das\*, Siddharth Goyal\*, Thibaut Lavril\*, Muhammed Shuaibi\*, Morgane Riviere, Kevin Tran, Javier Heras-Domingo, Caleb Ho, Weihua Hu, Aini Palizhati, Anuroop Sriram, Brandon Wood, Junwoong Yoon, Devi Parikh, C. Lawrence Zitnick, and Zachary Ulissi. Open catalyst 2020 (oc20) dataset and community challenges. *ACS Catalysis*, 0(0):6059–6072, 0. doi: 10.1021/acscatal.0c04525. URL <https://doi.org/10.1021/acscatal.0c04525>.
- [17] Deli Chen, Yankai Lin, Wei Li, Peng Li, Jie Zhou, and Xu Sun. Measuring and relieving the over-smoothing problem for graph neural networks from the topological view. *CoRR*, abs/1909.03211, 2019. URL <http://arxiv.org/abs/1909.03211>.
- [18] Deli Chen, Yankai Lin, W. Li, Peng Li, J. Zhou, and Xu Sun. Measuring and relieving the over-smoothing problem for graph neural networks from the topological view. In *AAAI*, 2020.
- [19] Stefan Chmiela, A. Tkatchenko, H. E. Sauceda, I. Poltavsky, Kristof T. Schütt, and K. Müller. Machine learning of accurate energy-conserving molecular force fields. *Science Advances*, 3, 2017.
- [20] J. Devlin, Ming-Wei Chang, Kenton Lee, and Kristina Toutanova. Bert: Pre-training of deep bidirectional transformers for language understanding. In *NAACL-HLT*, 2019.
- [21] David Duvenaud, Dougal Maclaurin, Jorge Aguilera-Iparraguirre, Rafael Gómez-Bombarelli, Timothy Hirzel, Alán Aspuru-Guzik, and Ryan P. Adams. Convolutional networks on graphs for learning molecular fingerprints. In *Proceedings of the 28th International Conference on Neural Information Processing Systems - Volume 2*, NIPS’15, page 2224–2232, Cambridge, MA, USA, 2015. MIT Press.
- [22] F. Fuchs, Daniel E. Worrall, Volker Fischer, and M. Welling. Se(3)-transformers: 3d rotation equivariant attention networks. *ArXiv*, abs/2006.10503, 2020.
- [23] J. Gilmer, S. Schoenholz, Patrick F. Riley, Oriol Vinyals, and George E. Dahl. Neural message passing for quantum chemistry. *ArXiv*, abs/1704.01212, 2017.
- [24] Jonathan Godwin\*, Thomas Keck\*, Peter Battaglia, Victor Bapst, Thomas Kipf, Yujia Li, Kimberly Stachenfeld, Petar Veličković, and Alvaro Sanchez-Gonzalez. Jraph: A library for graph neural networks in jax., 2020. URL <http://github.com/deepmind/jraph>.
- [25] Kaiming He, X. Zhang, Shaoqing Ren, and Jian Sun. Deep residual learning for image recognition. *2016 IEEE Conference on Computer Vision and Pattern Recognition (CVPR)*, pages 770–778, 2016.
- [26] Tom Hennigan, Trevor Cai, Tamara Norman, and Igor Babuschkin. Haiku: Sonnet for JAX, 2020. URL <http://github.com/deepmind/dm-haiku>.
- [27] Weihua Hu, Bowen Liu, Joseph Gomes, M. Zitnik, Percy Liang, V. Pande, and J. Leskovec. Strategies for pre-training graph neural networks. *arXiv: Learning*, 2020.
- [28] Weihua Hu, Muhammed Shuaibi, Abhishek Das, Siddharth Goyal, Anuroop Sriram, J. Leskovec, Devi Parikh, and C. L. Zitnick. Forcenet: A graph neural network for large-scale quantum calculations. *ArXiv*, abs/2103.01436, 2021.
- [29] Jared Kaplan, Sam McCandlish, Tom Henighan, Tom B. Brown, Benjamin Chess, Rewon Child, Scott Gray, Alec Radford, Jeffrey Wu, and Dario Amodei. Scaling laws for neural language models, 2020.
- [30] Diederik P. Kingma and Jimmy Ba. Adam: A method for stochastic optimization. *CoRR*, abs/1412.6980, 2015.
- [31] Johannes Klicpera, Shankari Giri, Johannes T. Margraf, and Stephan Günnemann. Fast and uncertainty-aware directional message passing for non-equilibrium molecules. *CoRR*, abs/2011.14115, 2020. URL <https://arxiv.org/abs/2011.14115>.

- [32] Johannes Klicpera, Janek Groß, and Stephan Günnemann. Directional message passing for molecular graphs. *ArXiv*, abs/2003.03123, 2020.
- [33] Risi Kondor, Hy Truong Son, Horace Pan, Brandon M. Anderson, and Shubhendu Trivedi. Covariant compositional networks for learning graphs. *CoRR*, abs/1801.02144, 2018. URL <http://arxiv.org/abs/1801.02144>.
- [34] Jonas Köhler, Leon Klein, and Frank Noé. Equivariant flows: sampling configurations for multi-body systems with symmetric energies, 2019.
- [35] Yann LeCun, Yoshua Bengio, and Geoffrey Hinton. Deep learning. *nature*, 521(7553):436–444, 2015.
- [36] G. Li, M. Müller, Ali K. Thabet, and Bernard Ghanem. Deepgcns: Can gcns go as deep as cnns? *2019 IEEE/CVF International Conference on Computer Vision (ICCV)*, pages 9266–9275, 2019.
- [37] Guohao Li, C. Xiong, Ali K. Thabet, and Bernard Ghanem. Deepergcn: All you need to train deeper gcns. *ArXiv*, abs/2006.07739, 2020.
- [38] Qimai Li, Zhichao Han, and Xiao-Ming Wu. Deeper insights into graph convolutional networks for semi-supervised learning. In *Proceedings of the AAAI Conference on Artificial Intelligence*, volume 32, 2018.
- [39] Yaping Liu, Limei Wang, Min Liu, Xuan Zhang, Bora Oztekin, and Shuiwang Ji. Spherical message passing for 3d graph networks. *ArXiv*, abs/2102.05013, 2021.
- [40] Razvan Pascanu, Tomas Mikolov, and Yoshua Bengio. On the difficulty of training recurrent neural networks. In *ICML*, 2013.
- [41] T. Pfaff, Meire Fortunato, Alvaro Sanchez-Gonzalez, and P. Battaglia. Learning mesh-based simulation with graph networks. *ArXiv*, abs/2010.03409, 2020.
- [42] R. Ramakrishnan, Pavlo O. Dral, M. Rupp, and O. A. von Lilienfeld. Quantum chemistry structures and properties of 134 kilo molecules. *Scientific Data*, 1, 2014.
- [43] Yu Rong, Wenbing Huang, Tingyang Xu, and Junzhou Huang. The truly deep graph convolutional networks for node classification. *CoRR*, abs/1907.10903, 2019. URL <http://arxiv.org/abs/1907.10903>.
- [44] Alvaro Sanchez-Gonzalez, N. Heess, Jost Tobias Springenberg, J. Merel, Martin A. Riedmiller, R. Hadsell, and P. Battaglia. Graph networks as learnable physics engines for inference and control. *ArXiv*, abs/1806.01242, 2018.
- [45] Alvaro Sanchez-Gonzalez, Jonathan Godwin, Tobias Pfaff, Rex Ying, Jure Leskovec, and Peter Battaglia. Learning to simulate complex physics with graph networks. In Hal Daumé III and Aarti Singh, editors, *Proceedings of the 37th International Conference on Machine Learning*, volume 119 of *Proceedings of Machine Learning Research*, pages 8459–8468. PMLR, 13–18 Jul 2020. URL <http://proceedings.mlr.press/v119/sanchez-gonzalez20a.html>.
- [46] Victor Garcia Satorras, Emiel Hoogeboom, and Max Welling. E(n) equivariant graph neural networks, 2021.
- [47] Franco Scarselli, Marco Gori, Ah Chung Tsoi, Markus Hagenbuchner, and Gabriele Monfardini. The graph neural network model. *IEEE Transactions on Neural Networks*, 20(1):61–80, 2009. doi: 10.1109/TNN.2008.2005605.
- [48] Kristof Schütt, Pieter-Jan Kindermans, Huziel Enoc Saucedo Felix, Stefan Chmiela, A. Tkatchenko, and K. Müller. Schnet: A continuous-filter convolutional neural network for modeling quantum interactions. In *NIPS*, 2017.
- [49] J. Sietsma and Robert J. F. Dow. Creating artificial neural networks that generalize. *Neural Networks*, 4:67–79, 1991.
- [50] Karen Simonyan and Andrew Zisserman. Very deep convolutional networks for large-scale image recognition. In *International Conference on Learning Representations*, 2015.

- [51] Shantanu Thakoor, C. Tallec, M. G. Azar, R. Munos, Petar Velivckovi'c, and Michal Valko. Bootstrapped representation learning on graphs. *ArXiv*, abs/2102.06514, 2021.
- [52] Nathaniel Thomas, Tess Smidt, Steven M. Kearnes, Lusann Yang, Li Li, Kai Kohlhoff, and Patrick Riley. Tensor field networks: Rotation- and translation-equivariant neural networks for 3d point clouds. *CoRR*, abs/1802.08219, 2018. URL <http://arxiv.org/abs/1802.08219>.
- [53] Oliver T. Unke and Markus Meuwly. Physnet: A neural network for predicting energies, forces, dipole moments, and partial charges. *Journal of Chemical Theory and Computation*, 15(6):3678–3693, May 2019. ISSN 1549-9626. doi: 10.1021/acs.jctc.9b00181. URL <http://dx.doi.org/10.1021/acs.jctc.9b00181>.
- [54] Pascal Vincent, H. Larochelle, Yoshua Bengio, and Pierre-Antoine Manzagol. Extracting and composing robust features with denoising autoencoders. In *ICML '08*, 2008.
- [55] Pascal Vincent, H. Larochelle, Isabelle Lajoie, Yoshua Bengio, and Pierre-Antoine Manzagol. Stacked denoising autoencoders: Learning useful representations in a deep network with a local denoising criterion. *J. Mach. Learn. Res.*, 11:3371–3408, 2010.
- [56] Zonghan Wu, Shirui Pan, Fengwen Chen, Guodong Long, Chengqi Zhang, and S Yu Philip. A comprehensive survey on graph neural networks. *IEEE transactions on neural networks and learning systems*, 2020.
- [57] Zonghan Wu, Shirui Pan, Fengwen Chen, Guodong Long, C. Zhang, and Philip S. Yu. A comprehensive survey on graph neural networks. *IEEE Transactions on Neural Networks and Learning Systems*, 32:4–24, 2021.
- [58] Chaoqi Yang, Ruijie Wang, Shuochao Yao, Shengzhong Liu, and Tarek Abdelzaher. Revisiting "over-smoothing" in deep gcns. *arXiv preprint arXiv:2003.13663*, 2020.
- [59] Yuning You, Tianlong Chen, Yongduo Sui, Ting Chen, Zhangyang Wang, and Yang Shen. Graph contrastive learning with augmentations. *ArXiv*, abs/2010.13902, 2020.
- [60] L. Zhao and Leman Akoglu. Pairnorm: Tackling oversmoothing in gnns. *ArXiv*, abs/1909.12223, 2020.
- [61] Jie Zhou, Ganqu Cui, Shengding Hu, Zhengyan Zhang, Cheng Yang, Zhiyuan Liu, Lifeng Wang, Changcheng Li, and Maosong Sun. Graph neural networks: A review of methods and applications. *AI Open*, 1:57–81, 2020.
- [62] Kuangqi Zhou, Yanfei Dong, Wee Sun Lee, Bryan Hooi, Huan Xu, and Jiashi Feng. Effective training strategies for deep graph neural networks. *CoRR*, abs/2006.07107, 2020. URL <https://arxiv.org/abs/2006.07107>.

## 8 Appendix

The following sections include details on training setup, hyper-parameters, input processing, as well as additional experimental results.

### 8.1 Analysis of Effect of Noisy Nodes.

In Figure F3 we analyse the impact of Noisy Nodes by plotting the Mean Absolute Distance (MAD) [18] of the residual updates of each layer. MAD is a measure of the diversity of graph node features, often used to quantify oversmoothing, the higher the number the more diverse the node features, the lower the number the less diverse. In this plot we can see that for Noisy Nodes the node updates remain diverse for all of the layers, whereas without noise the model makes very similar updates per node for the majority of layers.

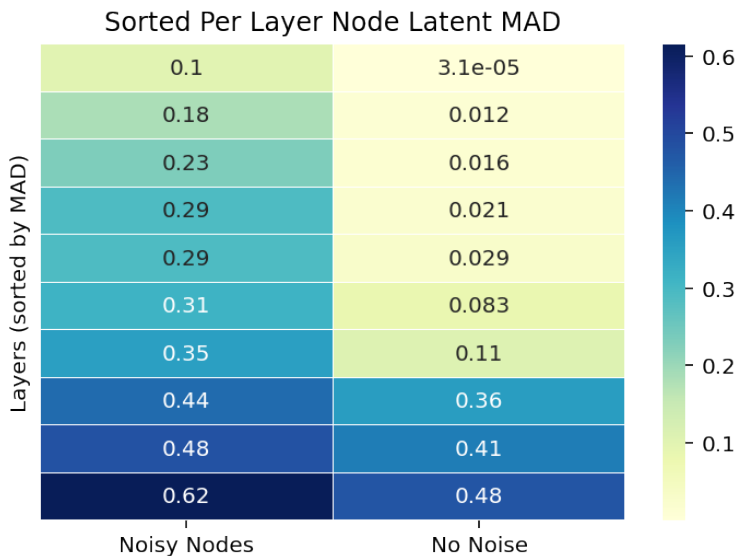


Figure 3: Residual Activation Per Layer, sorted by MAD. 10 Layer Model trained on QM9. We can see that Noisy Nodes encourages the model to make diverse residual updates per node. For Noisy Nodes all layers have a MAD above 0.1, compared to 4 for No Noise. In addition, half of the No Noise layers have MAD of below 0.05.

Table 7: OC20 IS2RS Test, Average Force below Threshold %,  $\uparrow$

Model	Method	OOD Both	OOD Adsorbate	OOD Catalyst	ID
Noisy Nodes	Direct	0.00%	0.00%	0.00%	0.63%
DimeNet ++	Relaxation	2.32%	3.01%	2.78%	3.69%

## 8.2 Additional Metrics for Open Catalyst IS2RS Test Set

Relaxation approaches to IS2RS minimise forces with respect to positions, with the expectation that forces at the minimum are close to zero. One metric of such a model’s success is to evaluate the forces at the converged structure using ground truth Density Functional Theory calculations and see how close they are to zero. Two metrics are provided by OC20 [16] on the IS2RS test set: Force below Threshold (FbT), which is the percentage of structures that have forces below 0.05 eV/Angstrom, and Average Force below Threshold (AFbT) which is FbT calculated at multiple thresholds.

However, force evaluation is arguably not a good metric of structural fidelity. Very small physical error at tiny inter-atomic distances can lead to an extremely large force error if atoms become too close together. Such a large force, caused by a very small positional error, would lead to failure on the force metrics even though the structures are very similar on distance measures. For this reason we do not report force metrics in the main body of the paper for our direct prediction results, since our positional model was not trained with any force data and we expect it to make such small positional errors. However, we present them here for completeness, since they are computed automatically upon submission.

The OC20 project computes test DFT calculations on the evaluation server and presents a summary result for all IS2RS position predictions. Such calculations take 10-12 hours and they are not available for the validation set. Thus, we are not able to analyse the results in Tables 7 and 8 in any further detail. Before application to catalyst screening further work may be needed for direct approaches to ensure forces do not explode from atoms being too close together.

Table 8: OC20 IS2RS Test, Force below Threshold %,  $\uparrow$ 

Model	Method	OOD Both	OOD Adsorbate	OOD Catalyst	ID
Noisy Nodes	Direct	0.0%	0.0%	0.0%	0.0%
DimeNet ++	Relaxation	0.0%	0.2%	0.2%	0.0%

### 8.3 Experiment setup

**Open Catalyst.** All training experiments were ran on a cluster of TPU devices. For the Open Catalyst experiments, each individual run (i.e. a single random seed) utilised 8 TPU devices on 2 hosts (4 per host) for training, and 4 V100 GPU devices for evaluation (1 per dataset).

Each Open Catalyst experiment was ran until convergence for up to 200 hours. Our best result, the large  $10 \times 10$  block-iterative model, requires 7 days of training using the above setting. Each configuration was run at least 3 times in this hardware configuration, including all ablation settings.

We further note that making effective use of our regulariser requires sweeping noise values. These sweeps are dataset dependent and can be carried out using few message passing steps (e.g. a single block iteration).

**QM9.** Experiments were also run on TPU devices. Each seed was run using 8 TPU devices on a single host for training, and 2 V100 GPU devices for evaluation. QM9 targets were trained between 12-24 hours per experiment.

Following [32] we define std. MAE as :

$$\text{std. MAE} = \frac{1}{M} \sum_{m=1}^M \left( \frac{1}{N} \sum_{i=1}^N \frac{|f_{\theta}^{(m)}(\mathbf{X}_i, \mathbf{z}_i) - \hat{t}_i^{(m)}|}{\sigma_m} \right)$$

and logMAE as:

$$\text{logMAE} = \frac{1}{M} \sum_{m=1}^M \log \left( \frac{1}{N} \sum_{i=1}^N \frac{|f_{\theta}^{(m)}(\mathbf{X}_i, \mathbf{z}_i) - \hat{t}_i^{(m)}|}{\sigma_m} \right)$$

with target index  $m$ , number of targets  $M = 12$ , dataset size  $N$ , ground truth values  $\hat{t}^{(m)}$ , model  $f_{\theta}^{(m)}$ , inputs  $\mathbf{X}_i$  and  $\mathbf{z}_i$ , and standard deviation  $\sigma_m$  of  $\hat{t}^{(m)}$ .

### 8.4 Hyper-parameters

**Open Catalyst.** We list the hyper-parameters used to train the default Open Catalyst experiment. If not specified otherwise (e.g. in ablations of these parameters), experiments were ran with this configuration.

Dynamic batch sizes refers to constructing batches by specifying maximum node, edge and graph counts (as opposed to only graph counts) to better balance computational load. Batches are constructed until one of the limits is reached.

Parameter updates were smoothed using an EMA for the current training step with the current decay value computed through  $decay = \min(decay, (1.0 + step)/(10.0 + step))$ . As discussed in the evaluation, best results on Open Catalyst were obtained by utilising 10 block iterations with 10 message passing layers.

**QM9** Table 10 lists QM9 hyper-parameters which primarily reflect the smaller dataset and geometries with fewer long range interactions.

Table 9: Open Catalyst training parameters.

Parameter	Value or description
Optimiser	Adam with warm up and cosine cycling
$\beta_1$	0.9
$\beta_2$	0.95
Warm up steps	$5e5$
Warm up start learning rate	$1e - 5$
Warm up/cosine max learning rate	$1e - 4$
Cosine cycle length	$5e6$
Loss type	Mean squared error
Batch size	Dynamic to max edge/node/graph count
Max nodes in batch	1024
Max edges in batch	12800
Max graphs in batch	10
MLP number of layers	3
MLP hidden sizes	512
Number Bessel Functions	512
Activation	shifted softplus
message passing layers	50
Block iterations	1
Node/Edge latent vector sizes	512
Position noise	Gaussian ( $\mu = 0, \sigma = 0.3$ )
Parameter update	Exponentially moving average (EMA) smoothing
EMA decay	0.9999
Position Loss Co-efficient	1.0

Table 10: QM9 training parameters.

Parameter	Value or description
Optimiser	Adam with warm up and cosine cycling
$\beta_1$	0.9
$\beta_2$	0.95
Warm up steps	$1e4$
Warm up start learning rate	$3e - 7$
Warm up/cosine max learning rate	$1e - 4$
Cosine cycle length	$2e6$
Loss type	Mean squared error
Batch size	Dynamic to max edge/node/graph count
Max nodes in batch	256
Max edges in batch	4096
Max graphs in batch	8
MLP number of layers	3
MLP hidden sizes	1024
Number Bessel Functions	512
Activation	shifted softplus
message passing layers	10
Block iterations	2
Node/Edge latent vector sizes	512
Position noise	Gaussian ( $\mu = 0, \sigma = 0.02$ )
Parameter update	Exponentially moving average (EMA) smoothing
EMA decay	0.9999
Position Loss Coefficient	0.1